10-2001

Crystal Structure of MtaN, a Global Multidrug Transporter Gene Activator

Michael H. Godsey
Oregon Health & Science University, mgodsey@cu-portland.edu

Natalya N. Baranova
University of Illinois at Chicago

Alexander A. Neyfakh
University of Illinois at Chicago

Richard G. Brennan
Oregon Health & Science University

Recommended Citation

Crystal Structure of MtaN, a Global Multidrug Transporter Gene Activator*

Michael H. Godsey‡, Natalya N. Baranova§, Alexander A. Neyfakh§, and Richard G. Brennan‡¶

From the ‡Department of Biochemistry and Molecular Biology, Oregon Health & Science University, Portland, Oregon 97201-3098 and the §Center for Pharmaceutical Biotechnology, University of Illinois, Chicago, Illinois 60607

MtaN (Multidrug Transporter Activation, N terminus) is a constitutive, transcriptionally active 109-residue truncation mutant, which contains only the N-terminal DNA-binding and dimerization domains of MerR family member Mta. The 2.75 Å resolution crystal structure of apo-MtaN reveals a winged helix-turn-helix protein with a protruding 8-turn helix (α5) that is involved in dimerization by the formation of an antiparallel coiled-coil. The hydrophobic core and helices α1 through α4 are structurally homologous to MerR family member BmrR bound to DNA, whereas one wing (Wing 1) is shifted. Differences between the orientation of α5 with respect to the core and the revolution of the antiparallel coiled-coil lead to significantly altered conformations of MtaN and BmrR dimers. These shifts result in a conformation of MtaN that appears to be incompatible with the transcription activation mechanism of BmrR and suggest that additional DNA-induced structural changes are necessary.

Bacterial multidrug resistance (MDR)[1] is a growing threat to human health. One key component of MDR is the efflux of structurally and chemically diverse compounds, including antibiotics, antiseptics, and disinfectants, by membrane-bound multidrug transporters (1, 2). Although often regulated by global regulators (3, 4) such as MarA (5), which activates over a dozen genes (6, 7), many MDR genes are regulated specifically, such as *qacA* by QacR (8) and *emrAB* by EmrR (9). In *Bacillus subtilis*, BmrR (10) and BltR (11), members of the MerR family (12), regulate transcription of the MDR transporter genes *bmr* and *blt*, respectively. MtaN (multidrug transporter activation, N terminus), another MerR family member, is a global activator of *B. subtilis* multidrug transporter genes and constitutively activates transcription of *bmr* and *blt*, another putative membrane protein gene (*ydfK*) and its own gene (13).

MerR proteins range from relatively small size, such as the

Escherichia coli MerR (144 residues per monomer) and *E. coli* ZntR (141 residues), to those over a hundred amino acid residues longer including *B. subtilis* BmrR (278 residues) or *Streptomyces lividans* TipAL (253 residues). These proteins form homodimers that regulate genes to combat a variety of cellular stresses. ZntR (14), CueR (15), PMTR (16), and MerR (12) bind divalent metal ions to activate their respective metal resistance systems, whereas SoxR responds to oxidative stress through redox disassembly of its iron-sulfur centers (17). NolA is involved in the nodulation process in *Bradyrhizobium japonicum* by responding to nodulation factors from soybeans (18). BmrR binds toxic lipophilic cations, although physiologically relevant ligand(s) of BmrR have yet to be identified (10). TipAL covalently binds the large antibiotic thiostrepton (19). Whereas MtaN is able to activate transcription of multidrug transporters and full-length Mta is closely related (40% sequence identity) to TipAL, Mta is not induced by thiostrepton (13), and the ligand or ligands of Mta remain unknown.

The N-terminal domain of each MerR subunit, the most conserved segment, contains a winged helix-turn-helix motif (20) and the dimerization region, which comprises half of an antiparallel coiled-coil (21). This ~110-residue domain is the signature of the MerR family, and it is likely to be structurally and functionally conserved. Beyond the winged helix-turn-helix motif, there appears to be no significant sequence or structural homology between MerR family members and other known gene regulators. The variable length C-terminal domain of MerR proteins contains ligand or coactivator binding elements that have been tailored to recognize their widely divergent and non-overlapping signals. Not surprisingly, the larger proteins bind larger coactivators, whereas the smaller proteins appear to be the minimum size necessary to respond to a divalent cation.

The function of the C terminus is to modulate the transcriptional activation of MerR family members by keeping the protein/DNA complex in a transcriptionally inactive form until a coactivator is bound, at which time repression is relieved, and the protein is able to up-regulate transcription (13, 22). MtaN is an unusual MerR family member because the protein lacks this modulation domain, which leads to its constitutive activation of cognate promoters (13). Because MtaN constitutively activates its own transcription, cells containing *mtaN* produce high levels of this protein through positive feedback. Eventually, elevated levels of MtaN overcome its lower affinities for the *bmr* and *blt* promoters, and those genes are activated (13). MtaN appears to represent the smallest active form of the MerR family of transcriptional regulators.

An unusual feature of the genes that are regulated by MerR family members is the 19-base pair (bp) separation of the −10 and −35 promoter elements (23), which is 17 bp in most bacterial promoters (24, 25). The 19-bp spacer appears to prevent open complex formation by RNA polymerase in the absence of

The atomic coordinates and structure factors (code 1JBG) have been deposited in the Protein Data Bank, Research Collaboratory for Structural Bioinformatics, Rutgers University, New Brunswick, NJ (http://www.rcsb.org/).

¶ To whom correspondence should be addressed. Tel.: 503-494-4427; Fax: 503-494-8393; E-mail: brennanr@ohsu.edu.

[1] The abbreviations used are: MDR, multidrug resistance; MtaN, multidrug transporter activation, N terminus; bp, base pair(s); r.m.s.d., root mean-squared deviation; MAD, multiwavelength anomalous diffraction; BmrR, bacterial multidrug resistance regulator.

This paper is available on line at http://www.jbc.org

TABLE I
Data and refinement statistics

Data Collection and MAD phasing statistics

Crystal	Native		Selenomethionine-substituted		
SSRL[a] Beamline	7–1		1–5		
Unit cell parameters (Å)	$a = 49.4$		$a = 50.1$		
	$b = 67.8$		$b = 67.6$		
	$c = 115.0$		$c = 116.1$		
Resolution limits (Å)	23.30–2.75		58.72–2.90		
Outer shell (Å)	2.82–2.75			2.98–2.90	
Wavelength (Å)	1.08	0.9226	0.97945	0.97988	1.06883
Observed reflections	42297	18,361	18,945	19,064	18,568
Unique reflections	5199	4502	4515	4523	4497
% Completeness (outer shell)	99.3 (99.0)	97.0 (100)	97.3 (100)	97.4 (100)	96.9 (93.5)
Mean $I/\sigma I$ (outer shell)	7.9 (2.7)	4.2 (1.4)	4.0 (1.5)	6.4 (1.6)	5.1 (2.0)
R_{sym} (%)[b] (outer shell)	7.2 (27.1)	6.7 (51.0)	6.8 (51.2)	5.3 (48.6)	5.1 (38.1)
MAD Figure of merit			0.688		

Refinement statistics (native data set)

Number of reflections (working/test)	4551/261
Number of nonhydrogen protein atoms	861
Solvent atoms	16
Resolution (Å)	25.0–2.75
R_{cryst}/R_{free} (%)	22.8/28.7
Bond length deviation (Å)	0.013
Bond angle deviation (°)	1.5
Average B-factor (Å²)	81.61

[a] Stanford Synchrotron Radiation Laboratory.

[b] $R_{sym} = \Sigma|I_O - I_{avg}|\Sigma I_O$.

an activator (23). This unusual promoter structure has led to a model of transcription regulation by these proteins in which activation is achieved by DNA distortion and untwisting (12, 26). The recent crystal structure of BmrR bound to DNA and coactivator has delineated a significant portion of the activation mechanism (27). The ternary complex shows that the center of the DNA-binding site is bent, untwisted, and bunched-up, shortening the effective length of the DNA and reconfiguring the RNA polymerase binding sites to resemble more closely a 17-bp spacer and allow open complex formation.

The BmrR-drug-DNA complex provides insight into one facet of transcription regulation by the MerR family. However, the extent of the conformational changes of these proteins needed to effect DNA binding and transcription activation, if any, are unknown. To address this aspect of the mechanism of MerR family transcription activation, we solved the crystal structure of MtaN to 2.75 Å resolution. Comparison of the structures of MtaN and DNA/drug-bound BmrR reveals their overall structural similarity, as well as significant tertiary and quaternary differences.

MATERIALS AND METHODS

Data Collection and Phase Determination—MtaN was expressed, purified, and crystallized as previously reported (22). Both multiwavelength anomalous diffraction (MAD) and native x-ray intensity data were collected on cryocooled crystals at −170 °C at the Stanford Synchrotron Radiation Laboratory (SSRL) on beamlines 1-5 and 7-1, respectively (22). Native intensity data were collected at $\lambda = 1.08$ Å. MAD data were collected from a selenomethionine-containing protein crystal at four wavelengths (Table I). Data were processed using MOSFLM (28). The structure of MtaN was determined by MAD phasing (29) as a special case of multiple isomorphous replacement (30). Three of five possible selenomethionine sites were located using SOLVE (31), and these revealed the space group to be $I2_12_12_1$. A fourth selenium site was located through difference Fourier analysis (22). The fifth possible site, the N-terminal methionine, was not found and likely cleaved during normal protein processing by *E. coli*. The four sites were refined and electron density maps calculated after density modification, including solvent flipping (63% estimated solvent) and histogram matching as implemented in CNS (32). The figure of merit for these phases increased from 0.69 in the initial MAD derived phases to 0.98 after density modification (resolution limit 58.0–2.9 Å). Initial electron density maps, calculated to 3.0 Å resolution, revealed a mostly α-helical

structure, sections of well connected backbone, and the locations of many side chains. The selenomethionine sites were later used to determine unambiguously the register of the protein chain.

Model Building and Refinement—An initial polyalanine trace was built manually to these maps with O (33). Iterative cycles of model building, including some side chains, with O and refinement with CNS continued until the usefulness of the MAD data was exhausted, at which point the MAD-derived model was used to solve the higher resolution native intensity data set by molecular replacement using EPMR (34). Refinement and model rebuilding were done alternately to fit the complete model using sigma A-weighted 2Fo-Fc and Fo-Fc maps (Fig. 6). Prior to refinement, 5% of the native data was set aside for cross-validation and R_{free} was used as a measure of the validity and progress of the model. Residues 2–107 are included in the final model but the final 2 residues of the protein, a 2-residue linker and the hexa-His tag are disordered and not included. The final R_{factor} and R_{free} are 0.227 and 0.287, respectively for data from 25.0–2.75 Å resolution. Four amino acids (residues Glu-67, His-71, Asn-73, and Lys-90) were refined as alanines because their side chain densities are missing or poor. The final model contains 16 solvent molecules. The stereochemistry of this structure was assessed with PROCHECK (35), which calculated 89% of all residues in the most favored region of the Ramachandran plot and none in the generously allowed or disallowed regions. Figs. 1, 2, 5, and 6 were produced with Swiss PDB viewer (50) and POV-ray (www.povray.org).

Alignment—An alignment of the amino acid sequences of ten members of the MerR family was performed using ClustalW (36) and aided by the structures of MtaN and BmrR. This alignment was examined using the computer programs Alscript (37) and AMAS (38). Functional conservation across the family was determined using a threshold value of 0.4 as described in the documentation of AMAS. Residues from the N terminus through residue 69 of MtaN were aligned simply and consistently, however when different parameters were entered into the ClustalW program, alignments C-terminal to residue 69 varied slightly and those presented in Fig. 3 represent its best fit. The alignment of BmrR to MtaN was confirmed by visual inspection of their structures. The coordinates and structure factor amplitudes have been deposited in the RCSB Protein Data Bank (accession code 1JBG).

RESULTS AND DISCUSSION

Overall Structure—The asymmetric unit contains a monomer of MtaN (Fig. 1). The electron density is clear for 106 residues; the C-terminal 10 aminoacyl residues (including the hexa-His tag) are missing, as is the N-terminal methionine, which was not seen in either the selenomethionine-substituted

FIG. 1. **A stereo view of the overall architecture of MtaN.** Every tenth residue is labeled.
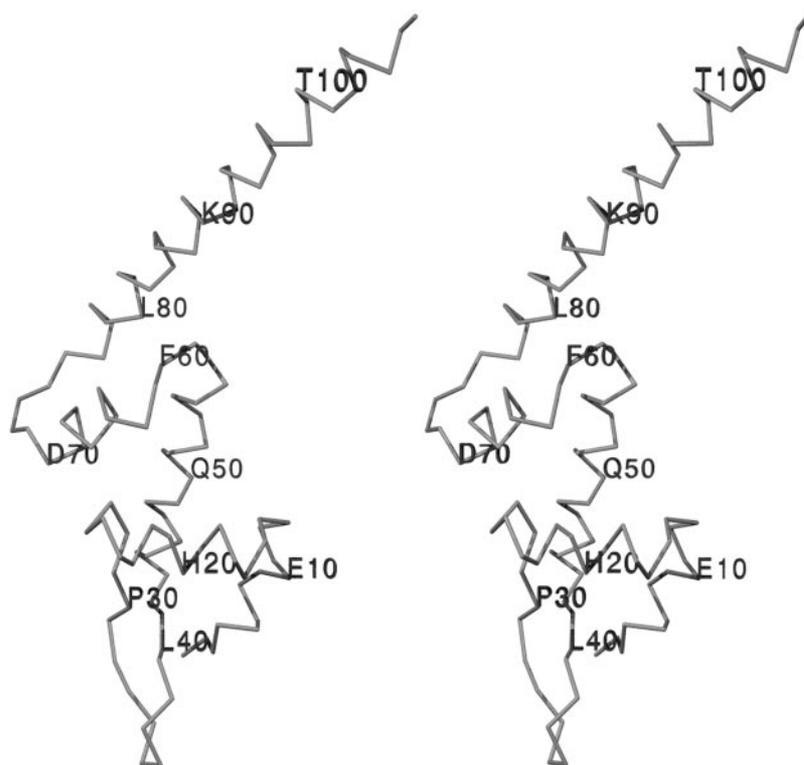
or native structures. The side chains of residues Glu-67, His-71, Asn-73, and Lys-90 are disordered and have been modeled as alanines.

The topological arrangement of secondary structural elements of MtaN begins with $\beta1$ (residues 2–4), followed by $\alpha1$ (residues 5–12) and $\alpha2$ (residues 16–24), which are connected by a 3-residue turn and comprise the conserved and predicted helix-turn-helix motif (20). Residues 25–31 form a loop that connects $\alpha2$ to strand $\beta2$ (residues 32–34), which is followed by a type II β-hairpin turn (residues 34–37) and strand $\beta3$ (residues 38–41). $\beta3$ is the center strand of a 3-stranded antiparallel β-sheet. A dipeptide connects $\beta3$ to helix $\alpha3$ (residues 43–58), which leads into a tight 3-residue turn that connects to helix $\alpha4$ (residues 62–70). A poorly structured loop (residues 71–75) connects the body ($\beta1$ through $\alpha4$) to a protruding 8-turn helix $\alpha5$ (residues 76–104). Thus, the topology of the MtaN monomer ($\beta1$-$\alpha1$-$\alpha2$-$\beta2$-$\beta3$-$\alpha3$-$\alpha4$-$\alpha5$) is the same as that of the N terminus of BmrR (27)(Fig. 2).

The monomer contains two functional domains: the N-terminal DNA-contacting domain from $\beta1$ to $\alpha4$ and the dimerization domain consisting of helix $\alpha5$ (Fig. 2). The DNA-binding domain is a member of the winged helix-turn-helix family of proteins (39), consisting of a four-helix bundle and a three-stranded antiparallel β-sheet. The dimerization domain consists of the 8-turn $\alpha5$ helix that forms a two-helix antiparallel coiled-coil with the other subunit. In BmrR $\alpha5$ contains three additional turns of helix that extend into the C-terminal domain. The strong conservation of this fold and that described for BmrR (28% sequence identity) confirms the hypothesis that this structure would be general for the MerR family.

DNA-binding Domain—The structure of MtaN is stabilized by a hydrophobic core, which consists of side chains from $\alpha1$ (Val-5, Val-8, Ala-9), $\alpha2$ (Leu-19, Tyr-22, Asp-23), $\beta3$ (Arg-39, Tyr-41), $\alpha3$ (Leu-46, Leu-49, Ile-52, Phe-55, Ile-58), and $\alpha4$ (Leu-62, Ile-65, Met-68, Leu-69) and turns between $\alpha1$ and $\alpha2$ (Val-14), $\alpha2$ and $\beta2$ (Ile-25, Leu-27, Leu-28, Pro-30), and $\alpha3$ and $\alpha4$ (Phe-60). All but 2 of these 23 core residues (Ile-25 and Pro-30) are well conserved across the MerR family (Fig. 3).

In addition to the hydrophobic component of the core, Asp-23 and Arg-39 form a buried salt bridge. This salt bridge buttresses the position of $\beta3$. In BmrR, this arginine (BmrR:Arg-43) is turned away from the carboxylate group of the aspartate (BmrR:Asp-26) to contact the DNA phosphate backbone. An Arg is absolutely conserved at this position across the MerR family and the Asp is either an Asp or Glu in all members but MerR, where it is a Gln. Whereas a formal possibility is that the Asp-23-Arg-39 salt bridge is in equilibrium with an un-bridged conformer, such as that seen in BmrR, the high ionic strength of the MtaN crystallization conditions (up to 5.0 M LiCl) would be expected to disfavor the formation of this observed salt bridge strongly. Given that Asp-23 and Arg-39 are found to interact in this environment indicates that this is a stable and physiologically relevant interaction. Thus this salt bridge interaction, and its subsequent DNA-induced breaking, is likely to be conserved in all MerR family members.

The reason for sequence conservation of MtaN and BmrR is clear. Of the body, defined as $\beta1$ through $\alpha4$, 26 of 69 MtaN and BmrR residues are identical, and of those 26, 15 are found in the core, and an additional 5 in turns. When conservative substitutions are included, the number of homologous residues rises to 36 and of those, 21 are found in the core. Thus, the observed sequence conservation between the two proteins ensures the structural conservation of this hydrophobic core. The same reasoning appears to apply across the whole family as these residues are among the most conserved in the N-terminal domain. Our analysis leads to the conclusion that DNA binding by MerR proteins does not significantly alter the structure of the hydrophobic core of the DNA-binding domains.

An overlay of Cα carbons of helices $\alpha1$ through $\alpha4$ of MtaN onto the corresponding BmrR atoms results in a root mean square (r.m.s.) deviation of 0.75 Å. That these four helices overlay so well suggests that either this domain of MtaN has taken the DNA-bound formation even in the absence of DNA, or more likely there is no difference in relative positions of these helices between the DNA-bound and free forms. However, residues Asp-47 and Ser-48 of BmrR $\alpha3$ are displaced

FIG. 2. **A ribbon diagram of the MtaN dimer.** One subunit is colored from *blue* at the N terminus to *red* at the C terminus. The other is colored *purple*. Secondary structural elements are labeled. The "body" domain includes $\beta1$, $\alpha1$, $\alpha2$, $\beta2$, $\beta3$, $\alpha3$, and $\alpha4$. The $\alpha5$ helices form the antiparallel coiled-coil.

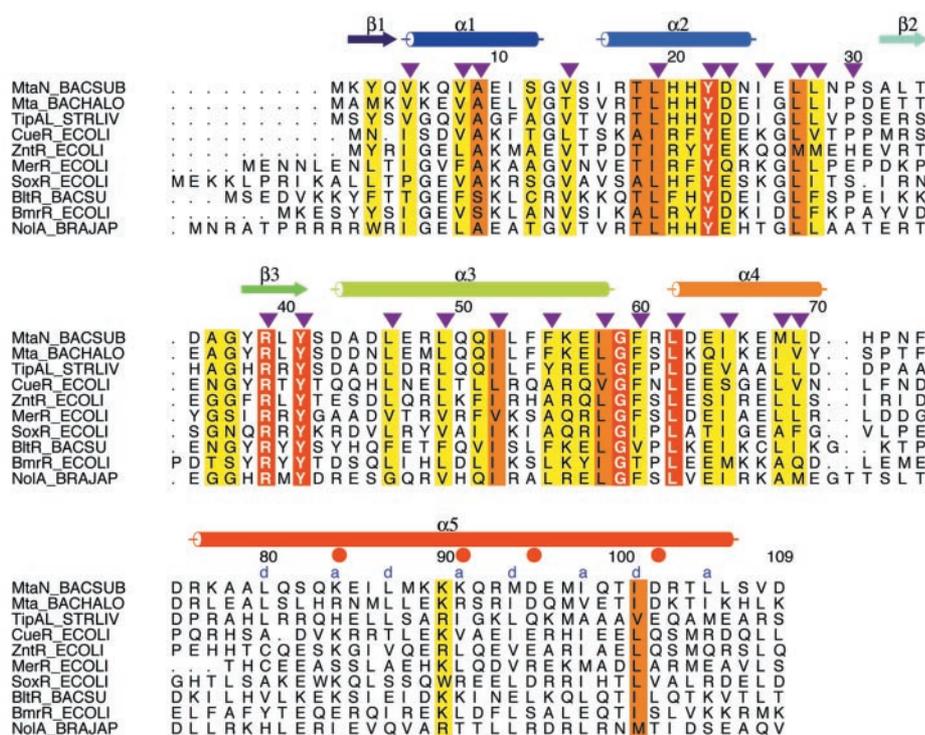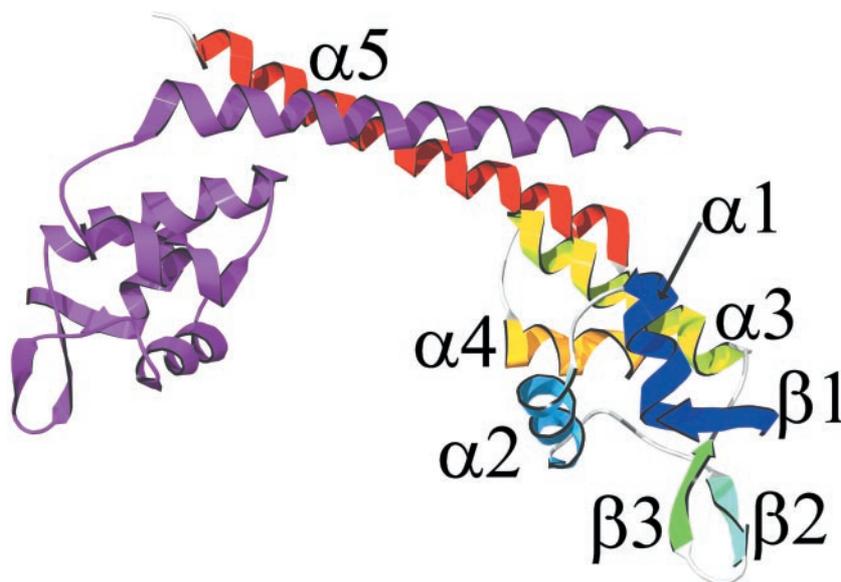FIG. 3. **A sequence alignment of MtaN and other MerR family members.** Conserved residues are color coded, with decreasing conservation from *red shading* (absolute) to *white* (more variable). The secondary structure elements of MtaN are shown above the alignment and colored as in Fig. 2. *Purple arrowheads* denote residues with side chains contributing to the core. *Filled red circles* are MtaN residues involved in intermolecular salt-bridges. The a and d positions of the antiparallel coiled-coil are indicated.

from their MtaN counterparts (Asp-43 and Ala-44) by their connection to the β-sheet, which takes a different conformation, and by their direct interaction with the drug-binding domain of BmrR, which is not present in MtaN.

Whereas the cores of MtaN and BmrR and the positions of the body helices ($\alpha1$-$\alpha4$) are the same, a structural difference is evident in the position of Wing 1 ($\beta2$-turn-$\beta3$). Specifically, MtaN displays a type II β-turn (Thr-34-Gly-37), whereas BmrR does not contain this classic hairpin because of a single residue insertion in this area, and is thus better described as a small loop. In addition, MtaN Wing 1 makes crystal lattice contacts, whereby Tyr-38 stacks against a symmetry-related Tyr-38. In BmrR this residue (BmrR:Tyr-42) interacts with a base in the minor groove. As a result, the Cα of Asp-35 (BmrR:Asp-39), which is located at the crux of the β-turn, moves 8.3 Å. Either interaction (protein-protein or protein-DNA) might be enough to displace the end of this β-sheet and therefore, Wing 1. Such

wing flexibility is well documented in other winged-helix proteins (40, 41). Regardless of its position in the current structure, Tyr-38 is likely to be involved in DNA binding by MtaN as well. The more global shift in the rest of the wing is more likely because of the absence of DNA and the different interactions of conserved residue Arg-39, which forms a salt bridge to Asp-23 in MtaN and a DNA backbone contact in BmrR (BmrR:Arg-43).

Dimerization Domain—The MtaN dimer is stabilized primarily by the formation of an antiparallel coiled-coil between the amphipathic $\alpha5$ helices. Coiled-coils are characterized by a heptad repeat $(abcdefg)_n$ in which the a and d positions are typically occupied by hydrophobic residues and form the interface between the interacting helices (42, 43). In MtaN, the hydrophobic core of the interface consists of the side chains of residues Leu-80 ($d1$), Leu-87 ($d2$), Met-94 ($d3$), Ile-98 ($a3$), Ile-101 ($d4$) and Leu-105 ($a4$), and the methylene carbons of Lys-84 ($a1$) and Lys-91 ($a2$). In the antiparallel conformation

FIG. 4. **A schematic diagram of the antiparallel coiled-coil of MtaN.** Intersubunit salt bridges between the *a* and *e* positions are depicted by *gray lines*. Residues at the *a* and *d* positions form the hydrophobic core of the interacting helices.
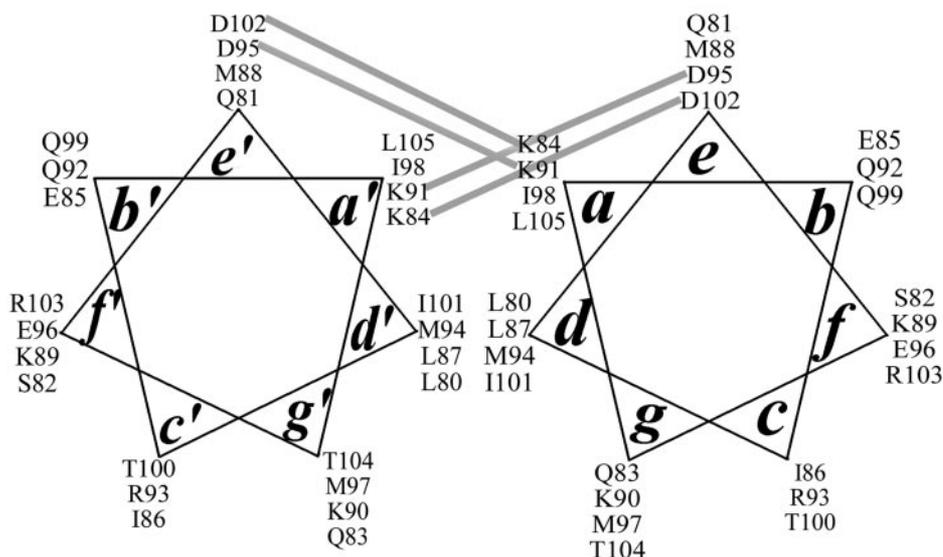
found in MtaN, van der Waals contacts are from *d*1 to *a*4′, *a*1 to *d*4′, *d*2 to *a*3′, *a*2 to *d*3′, (where ′ indicates the dimer partner) as well as the symmetry imposed interactions (Fig. 4). In addition to forming the antiparallel coiled-coil, the C-terminal end of the α5 helix also interacts with the C terminus of α3′. Contacts are found between the side chain of Phe-54 and Cγ of Thr-104′, and the alkyl side chains of Ile-58 and Ile-101′. van der Waals contacts between Glu-57 and Met-97′ complete the dimerization interface. Dimerization buries 738 Å^2 of accessible surface area per monomer, which is average for many oligomeric proteins (44).

Beyond the hydrophobic interactions, two *a* residues of MtaN, Lys-84 and Lys-91 and their dyadic mates, form salt bridges to Asp-102′ and Asp-95′, respectively, whereas the corresponding BmrR residues do not. Interhelix ionic interactions are common among both parallel and antiparallel coiled-coils and serve to stabilize the dimer and prevent unwanted heterodimerization (45, 46). Heterodimerization has not been observed between MerR family members.

An antiparallel coiled-coil was first indicated in MerR (47–49) and predicted to occur in all MerR family members (21), which was confirmed by the structure determination of BmrR. In both MtaN and BmrR, all *d* positions are occupied by hydrophobic residues, whereas their *a* positions vary significantly (Fig. 4). Specifically, at MtaN *a* positions Lys-91, Ile-98, and Leu-105, the respective BmrR residues are Leu, Glu, and Lys. Where both proteins have hydrophilic *a* residues they are oppositely charged (MtaN:Lys-84, BmrR:Glu-88). Overall, the buried residues of the coiled-coil (80 through 105) are only partially conserved across the family, even between MtaN and TipAL, the most closely related MerR protein (13) (49% sequence identity). Only residues corresponding to Ile-101, which is always hydrophobic, and Leu-80, Leu-87, Met-94, and Ile-98, which are usually hydrophobic, are reasonably conserved (Fig. 3). Thus, the variation of buried residues serves to stabilize the dimer and contributes to the prevention of heterodimerization.

Conformational Differences between Two MerR Family Members—An overlay of the conserved four-helix core of one monomer of MtaN onto the corresponding core of DNA-bound BmrR revealed a significant shift in the relative positions of the recognition helix (α2′) of the other subunit (Fig. 5). In MtaN the center-to-center distance of these helices is 33.3 Å, close to the 34 Å repeat distance of canonical B-form DNA and consistent with their binding to consecutive major grooves. In the
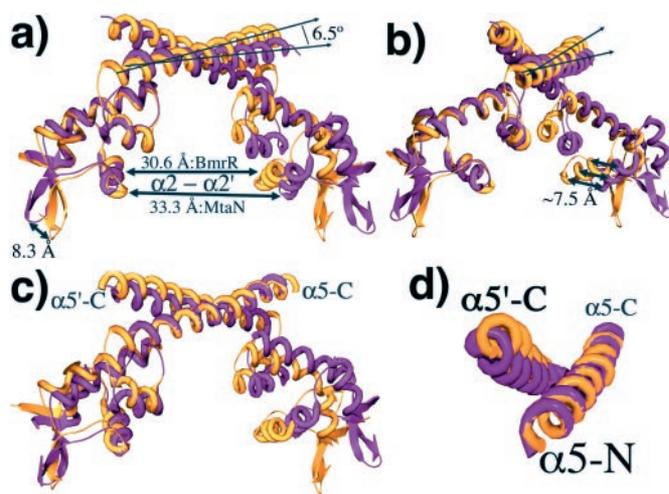

FIG. 5. **Conformational differences between MtaN and BmrR.** MtaN is in *purple* and the first 110 residues of BmrR are in gold. *a*, superimposition of helices α1 through α4 (*left monomers*) reveals the rotation of the α5 helix, altered positions of the β-sheets and different orientations of the α2 and α2′ helices, which in MtaN are farther apart and rotated counterclockwise. *b*, a view of the same overlay in *a* rotated by ~45°. This view highlights the different locations of the MtaN and BmrR α2′ helices, which are shifted ~7.5 Å. *c*, superimposition of the α5 helices. The α5′ C-terminal end of BmrR is revolved around the overlaid α5 helices as compared with MtaN, resulting in a large shift in the body of the dimer partner and a smaller effect on the position of the monomer body. *d*, the same overlay as *c*, but looking at the N terminus of α5 and C terminus of α5′. The remainder of the protein has been deleted for clarity.

transcription-activated conformation of BmrR these helices are only 30.6 Å apart, which corresponds to their major-groove binding to a shortened and undertwisted DNA double helix (27). In addition to the distances, the relative positions of these helices have changed with respect to each other. The resulting position of the MtaN α2′ is offset from the BmrR α2′ by 7.5 Å, largely because of the lateral twist of 15° of the dimer partner, rather than a simple direct lengthening between the major groove binding helices (Fig. 5, *a* and *b*).

The rotation between subunits is the result of two conformational changes that occur in the antiparallel coiled-coil. When MtaN and BmrR helices α1 through α4 are overlaid, a shift in the relative positions of their α5 helices is evident (Fig. 5, *a* and

FIG. 6. **A stereo view of sigma A-weighted-simulated annealing (2Fo-Fc) omit map electron density in the area of the β-turn between β2 and β3, contoured at 1σ.**
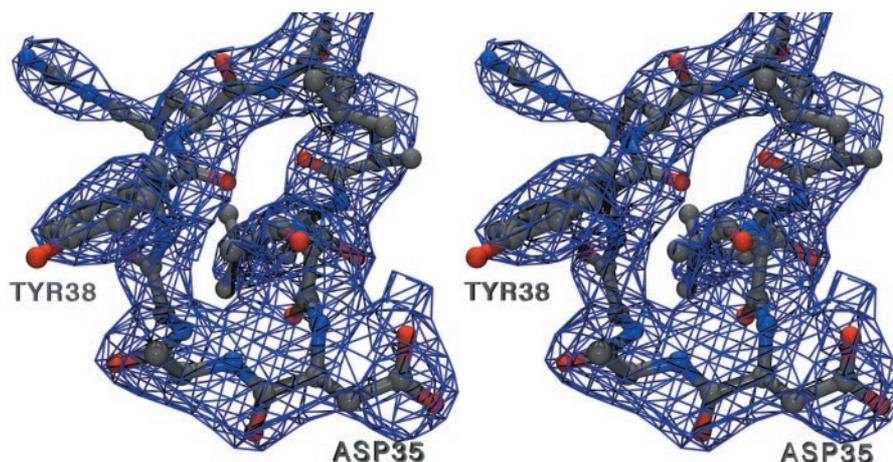
b). In comparison to MtaN α5, the BmrR α5 has rotated ~6.5° up and away. The body of the dimer partner moves to match this relocation to maintain the contacts between helices α5 and α3′. This relatively small rotation is doubled by the same rotation of the dimer partner, and further amplified by the length of the coiled-coil. In addition to the rotation of the α5 helix, the relative conformations of the antiparallel coiled-coils of MtaN and BmrR are different. When α5 of MtaN is overlaid onto the α5 of BmrR (r.m.s. deviation is 0.63 Å for the Cα carbons), the α5′ helices do not overlay (Fig. 5, *c* and *d*). Rather, the C-terminal end of the MtaN α5′ helix has revolved ~15° in a counter-clockwise direction around the overlaid α5 helices. The movement of the N terminus of α5′ helix is smaller, but changes the direction of the helical axis to match the revolution that occurs at the C-terminal end. This revolution rotates the body, *i.e.* the DNA-binding domain, of the dimer partner around the axis of the coiled-coil and swings it toward the other body domain, thereby accounting for the observed expansion of the recognition helices of MtaN.

DNA-induced Conformational Changes—MtaN is a constitutive activator, yet the dimer structures of MtaN and BmrR, the latter of which is in its transcription-activated conformation, are different. Perhaps the differences reflect dissimilar DNA-binding modes in which MtaN twists its promoter DNA to a lesser degree. Alternatively, the DNA binding site might play a role in the induction of additional conformational changes in MtaN so that it more closely resembles BmrR.

DNA-docking experiments reveal that the MtaN dimer is unable to bind the BmrR-activated DNA (27) because its α2 major groove recognition helices are too far apart and in the wrong orientation to fit into the major grooves (Fig. 5). MtaN is also unable to bind canonical B-form DNA because the α2 helices are tilted incorrectly to fit directly into adjacent major grooves and Wing 1 clashes with the DNA backbone. Thus at the least, MtaN requires minor structural adjustment in the twist of its α2 helices and more significant changes in the position of its β-sheet (Wing 1) to bind either DNA conformation (Figs. 5 and 6).

Given the results of our docking experiments a binding and activation mechanism can be envisioned. In this proposal the first step is MtaN binding to a B-like DNA conformation. This would likely be concomitant with or followed by the breaking of the Asp-23–Arg-39 salt bridge. The disruption would allow Arg-39 to contact the DNA phosphate backbone, perhaps as observed in the BmrR-*bmr* promoter complex (27) and remove a key constraint that holds MtaN in a non-activating conformation. Additional structural changes would be transmitted through the coiled-coil and allow the MtaN conformation to maximize its DNA contacts. This in turn could elicit DNA

conformational changes, which would result in an activated conformation of the MtaN-*mta* promoter complex that would more closely resemble that of the BmrR-*bmr* complex. The structure of an MtaN-*mta* promoter complex should provide more understanding of the DNA-binding and transcription activation mechanisms of this MerR family member.

REFERENCES

1. Paulsen, I. T., Brown, M. H., and Skurray, R. A. (1996) *Microbiol. Rev.* **60**, 575–608
2. van Veen, H. W., Putman, M., Margolles, A., Sakamoto, K., and Konings, W. N. (1999) *Biochim. Biophys. Acta* **1461**, 201–206
3. Grkovic, S., Brown, M. H., and Skurray, R. A. (2001) *Semin Cell Dev. Biol.* **12**, 225–237
4. Putman, M., van Veen, H. W., and Konings, W. N. (2000) *Microbiol. Mol. Biol. Rev.* **64**, 672–693
5. Rhee, S., Martin, R. G., Rosner, J. L., and Davies, D. R. (1998) *Proc. Natl. Acad. Sci. U. S. A.* **95**, 10413–10418
6. Alekshun, M. N., and Levy, S. B. (1997) *Antimicrob. Agents Chemother.* **41**, 2067–2075
7. Barbosa, T. M., and Levy, S. B. (2000) *J. Bacteriol.* **182**, 3467–3474
8. Grkovic, S., Brown, M. H., Roberts, N. J., Paulsen, I. T., and Skurray, R. A. (1998) *J. Biol. Chem.* **273**, 18665–18673
9. Lomovskaya, O., Lewis, K., and Matin, A. (1995) *J. Bacteriol.* **177**, 2328–2334
10. Ahmed, M., Borsch, C. M., Taylor, S. S., Vazquez-Laslop, N., and Neyfakh, A. A. (1994) *J. Biol. Chem.* **269**, 28506–28513
11. Ahmed, M., Lyass, L., Markham, P. N., Taylor, S. S., Vazquez-Laslop, N., and Neyfakh, A. A. (1995) *J. Bacteriol.* **177**, 3904–3910
12. Summers, A. O. (1992) *J. Bacteriol.* **174**, 3097–3101
13. Baranova, N. N., Danchin, A., and Neyfakh, A. A. (1999) *Mol. Microbiol.* **31**, 1549–1559
14. Outten, C. E., Outten, F. W., and O'Halloran, T. V. (1999) *J. Biol. Chem.* **274**, 37517–37524
15. Outten, F. W., Outten, C. E., Hale, J., and O'Halloran, T. V. (2000) *J. Biol. Chem.* **275**, 31024–31029
16. Noll, M., Petrukhin, K., and Lutsenko, S. (1998) *J. Biol. Chem.* **273**, 21393–21401
17. Hidalgo, E., Ding, H., and Demple, B. (1997) *Trends Biochem. Sci.* **22**, 207–210
18. Sadowsky, M. J., Cregan, P. B., Gottfert, M., Sharma, A., Gerhold, D., Rodriguez-Quinones, F., Keyser, H. H., Hennecke, H., and Stacey, G. (1991) *Proc. Natl. Acad. Sci. U. S. A.* **88**, 637–641
19. Holmes, D. J., Caso, J. L., and Thompson, C. J. (1993) *EMBO J.* **12**, 3183–3191
20. Shewchuk, L. M., Helmann, J. D., Ross, W., Park, S. J., Summers, A. O., and Walsh, C. T. (1989) *Biochemistry* **28**, 2340–2344
21. Caguiat, J. J., Watson, A. L., and Summers, A. O. (1999) *J. Bacteriol.* **181**, 3462–3471
22. Godsey, M. H., Baranova, N. N., Neyfakh, A. A., and Brennan, R. G. (2000) *Acta Crystallogr. Sect. D* **56**, 1456–1458
23. Parkhill, J., and Brown, N. L. (1990) *Nucleic Acids Res.* **18**, 5157–5162
24. Helmann, J. D. (1995) *Nucleic Acids Res.* **23**, 2351–2360
25. McClure, W. R. (1985) *Annu. Rev. Biochem.* **54**, 171–204
26. Ansari, A. Z., Chael, M. L., and O'Halloran, T. V. (1992) *Nature* **355**, 87–89
27. Zheleznova-Heldwein, E. E., and Brennan, R. G. (2001) *Nature* **409**, 378–382

28. Leslie, A. G. W. (1992) *Joint CCP4 + ESF-EAMCB Newsletter on Protein Crystallography*, Vol. 26
29. Hendrickson, W. A. (1991) *Science* **254,** 51–58
30. Ramakrishnan, V., and Biou, V. (1997) *Methods Enzymol.* **276,** 538–557
31. Terwilliger, T. C., and Berendzen, J. (1999) *Acta Crystallogr. Sect. D* **55,** 849–861
32. Brunger, A. T., Adams, P. D., Clore, G. M., DeLano, W. L., Gros, P., Grosse-Kunstleve, R. W., Jiang, J. S., Kuszewski, J., Nilges, M., Pannu, N. S., Read, R. J., Rice, L. M., Simonson, T., and Warren, G. L. (1998) *Acta Crystallogr. Sect. D* **54,** 905–921
33. Jones, T. A., Zou, J. Y., Cowan, S. W., and Kjeldgaard. (1991) *Acta Crystallogr. Sect. A* **47,** 110–119
34. Kissinger, C. R., Gehlhaar, D. K., and Fogel, D. B. (1999) *Acta Crystallogr. Sect. D* **55,** 484–491
35. Laskowski, R. A., MacArthur, M. W., Moss, D. S., and Thornton, J. M. (1993) *J. Appl. Cryst.* **26,** 283–291
36. Thompson, J. D., Higgins, D. G., and Gibson, T. J. (1994) *Nucleic Acids Res.* **22,** 4673–4680
37. Barton, G. J. (1993) *Protein Eng.* **6,** 37–40
38. Livingstone, C. D., and Barton, G. J. (1993) *Comput. Appl. Biosci.* **9,** 745–756
39. Gajiwala, K. S., and Burley, S. K. (2000) *Curr. Opin. Struct. Biol.* **10,** 110–116
40. Jin, C., and Liao, X. (1999) *J. Mol. Biol.* **292,** 641–651
41. Jin, C., Marsden, I., Chen, X., and Liao, X. (1999) *J. Mol. Biol.* **289,** 683–690
42. Nishikawa, K., and Scheraga, H. A. (1976) *Macromolecules* **9,** 395–407
43. Fujinaga, M., Berthet-Colominas, C., Yaremchuk, A. D., Tukalo, M. A., and Cusack, S. (1993) *J. Mol. Biol.* **234,** 222–233
44. Conte, L. L., Chothia, C., and Janin, J. (1999) *J. Mol. Biol.* **285,** 2177–2198
45. Zhou, N. E., Kay, C. M., and Hodges, R. S. (1994) *J. Mol. Biol.* **237,** 500–512
46. Monera, O. D., Kay, C. M., and Hodges, R. S. (1994) *Biochemistry* **33,** 3862–3871
47. Zeng, Q., Stalhandske, C., Anderson, M. C., Scott, R. A., and Summers, A. O. (1998) *Biochemistry* **37,** 15885–15895
48. Lupas, A. (1997) *Curr. Opin. Struct. Biol.* **7,** 388–393
49. Wolf, E., Kim, P. S., and Berger, B. (1997) *Protein Sci.* **6,** 1179–1189
50. Guex, N., and Peitsch, M. C. (1997) *Electrophoresis* **18,** 2714–2723